applied sciences

Article

Numerical Simulation Analysis of the Influence of Interlayer Quantity on the Long-Term Stable Operation of Gas Storage Facilities

Lilong Li [1], Xin Jiang [2], Jiafeng Tan [3,*], Rong Liu [4,*], Xiaolinag Quan [1], Jinyang Fan [3], Cheng Qian [2] and Jinjie Suo [3]

1 Sichuan Yanjiang Yijin Expressway Co., Ltd., Xichang 615099, China; zebra-2000@163.com (L.L.); quanxliang@163.com (X.Q.)
2 Chongqing Chengtou Jiangchang Construction Co., Ltd., Chongqing 400023, China; jxeent@163.com (X.J.); qianchengqc@foxmail.com (C.Q.)
3 School of Resources and Safety Engineering, Chongqing University, Chongqing 400044, China; jinyang.f@cqu.edu.cn (J.F.); 202120021018@stu.cap.edu.cn (J.S.)
4 Institute of Future Civil Engineering Science and Technology, Chongqing Jiaotong University, Chongqing 400074, China
* Correspondence: 202320021058t@stu.cqu.edu.cn (J.T.); cqu_liurong@163.com (R.L.); Tel.: +86-13628232903 (J.T.); +86-17783002935 (R.L.)

Abstract: Salt rock is considered as an ideal energy storage medium, and compressed air energy storage by a salt cavern can improve the utilisation efficiency of renewable energy. Salt rock in China mostly contains different interlayers, among which mudstone interlayers are the most common. At present, there are relatively few studies on the influence of mudstone interlayers on the long-term stable operation of gas storage. FLAC3D software was used to simulate the long-term operation of salt rock gas storage with different numbers of interlayers in the Yexian area of Pingdingshan. The results show that with the passage of time, the vertical displacement of the surrounding rock of the vertical single-cavity gas storage tank increases gradually. The maximum settlement value at the top of the surrounding rock is always greater than the maximum uplift value at the bottom. The horizontal displacement shows obvious symmetry with the vertical displacement at the top and bottom of the surrounding rock. The effect of the cyclic pressure interval on horizontal displacement is the same as that of vertical displacement. With the increase in the number of interlayers, the volume of the plastic zone gradually increases with the increase in the running time, and the increasing speed shows a growing trend.

Keywords: salt cavern; mudstone interlayer; FLAC3D; simulation

Citation: Li, L.; Jiang, X.; Tan, J.; Liu, R.; Quan, X.; Fan, J.; Qian, C.; Suo, J. Numerical Simulation Analysis of the Influence of Interlayer Quantity on the Long-Term Stable Operation of Gas Storage Facilities. *Appl. Sci.* **2024**, *14*, 9760. https://doi.org/10.3390/app14219760

Academic Editor: Andrea Frazzica

Received: 20 August 2024
Revised: 4 October 2024
Accepted: 8 October 2024
Published: 25 October 2024

1. Introduction

Salt rock is regarded as an optimal medium for energy storage, given its favourable rheological properties, low porosity, low permeability, and damage self-healing attributes. The utilisation of salt caverns for compressed air energy storage has emerged as an efficacious methodology for enhancing the utilisation efficiency of renewable energy. The characteristics of a foreign salt cavern's underground gas storage include a shallow burial, a large stratum thickness, high-grade salt rock, and a minimal number of interlayers. However, the buried salt mine in China is typically situated at greater depths, exceeding 2000 m in certain regions. The rock layer in these mines is relatively thin, ranging from 60 to 250 m in thickness. Additionally, the salt rock in Chinese mines is predominantly layered, comprising up to eight layers of thicker interlayers [1–3]. The mudstone interlayer is particularly prevalent, representing a significant portion of the rock composition.

In light of the increasingly severe global climate crisis, it is imperative that China prioritises the utilisation of renewable energy sources in order to achieve its dual-carbon objective. According to estimates, to reach carbon neutrality by 2060, clean energy should account for about 60 percent of the country's energy consumption [4]. The large-scale utilisation of salt cavern space gives full play to its advantages of a large capacity, cleanliness, environmental protection, safety, reliability, and economy, and provides important support for reaching national strategic objectives [5]. However, due to the layered structure of Chinese salt rocks, which is different from that of foreign countries, the presence of interlayers and impurities poses a serious threat to the safety of the reservoirs [6]. In order to guarantee the secure operation of salt cavern gas storage reservoirs, a considerable number of scholars have conducted research on the salt rocks. However, there has been comparatively little investigation into the mudstone interlayers present within the reservoirs.

Taheri et al. [7] found that creep of Gachsaran rock salt shows strong sensitivity to temperature changes; however, its sensitivity to different stress changes is low. Zhao K. et al. [8] investigated the creep fatigue characteristics of salt rock under different loading and unloading paths, and explained the deformation behaviour from the perspective of microscopic mechanisms. Malinjian et al. [9] employed a nonlinear cumulative damage rule to predict the cyclic life of rock salt under creep-fatigue loading. Hakan et al. [10] studied the creep behaviour of salt rocks and proposed a mathematical model that can explain their creep behaviour. Wang Junbao et al. [11] studied the creep characteristics of salt rock under low-frequency cyclic loading, and obtained the axial creep equation of Burgers' model under cyclic loading. By comparing the fatigue characteristics of salt rock in intermittent fatigue tests with those of salt rock without intermittent fatigue tests, Jiang Deyi et al. [12] found that the fatigue life of salt rock was shortened under intermittent action. Fan Jinyang et al. [13] proposed an intrinsic model of creep fatigue in salt rock based on hardening coefficients. Li Zongze et al. [14] investigated the effects of different circumferential pressures and stress levels on the interval fatigue of salt rock, and found that the presence of circumferential pressure enhanced the compressive strength of salt rock while increasing the fatigue life. Cui Yao et al. [15] investigated the acoustic emission characteristics of salt rock through intermittent fatigue tests, further revealing the effect of the time interval on the residual strain and fatigue life of salt rock. The evolution of rock salt deformation and elastic constants under the influence of time interval factors was investigated by Li Xin et al. [16]. By summarising a large amount of the literature on salt rock creep tests, Bingren Hou et al. [17] found that under constant axial pressure and cyclic peripheral pressure paths, the creep properties of salt rocks are significantly affected by the peripheral pressure and cyclic cycle.

In addition, a large number of scholars have studied the factors affecting the stability of salt cavern cavities for the safe and stable operation of salt cavern gas storage reservoirs. Yu Haibing et al. [18] studied the influence law of salt layer inclination and burial depth on the deformation and volume contraction of the salt cavity, and gave the safe mining depth of the proposed salt mine. Liang Wuxing et al. [19] combined Ansys and FLAC3D to carry out numerical simulation, and judged that the effect of three factors on the stability of the cavity based on the results of linear fitting was cavity burial depth > pressure interval > pressure difference. Fu Xing et al. [20] used FLAC3D 3.00 software to analyse the long-term operational stability of energy storage cavities in order to discuss the possibility of the safe operation of CAES reservoirs under Chinese domestic stratigraphic conditions. Liu Wei et al. [21] conducted permeability tests based on interface-bearing salt rocks from domestic salt mines, and numerical simulations based on the test results on the stability and confinement of natural gas reservoirs containing entrapped underground salt caverns. Zhixin Zhang et al. [22] conducted a series of indoor tests, theoretical and numerical simulations, and discussions to simulate hydrogen leakage from cave chambers under different conditions using COMSOL Multiphysics 6.0 software, and analysed the leakage range, pore pressure, and the amount of hydrogen leakage. Chunhe Yang et al. [23] combined the stability characteristics of salt caverns and gave five key scientific and technological issues facing the deep large-scale salt cavern energy storage technology in China. Tongtao Wang et al. [24] explored the effects of different gas frequencies on the stability of horizontal salt caverns under different geological conditions. They found that shallow salt caverns are suitable for compressed air energy storage, medium and deep salt caverns are suitable for natural gas energy storage, and deep salt caverns are suitable for helium energy storage. Leszek Lankof et al. [25] discussed the suitability of underground hydrogen storage facilities in layered salt caverns based on a geographic information system (GIS), taking into account the results of previous studies on the storage capacity of rock salt deposits.

This paper presents a study of the salt cavern gas storage reservoir in the Yexian area of the Pingdingshan Mountain. The research employs a comprehensive approach combining theoretical analysis and numerical simulations to investigate the impact of varying numbers of interlayers on the long-term stability of the gas storage reservoir. The objective is to address the research gap concerning mudstone interlayers and to provide theoretical support and numerical simulation analyses for the safe operation of gas storage reservoirs.

2. Materials and Methods

2.1. Introduction to FLAC3D Finite Difference Software

FLAC is an acronym that stands for "Fast Lagrangian Analysis of Continua". It is a computer program designed for the numerical modelling and simulation of geotechnical and rock mechanics problems. The FLAC program employs a finite difference method to simulate the mechanical behaviour of continuous media in a discrete form. This includes processes such as deformation, fracture, and stress transfer in rocks. The software is frequently employed to model a range of problems in diverse fields, including rock engineering, groundwater flow, earthquake geology, and underground storage. FLAC is a frequently utilised finite element software in the domain of geotechnical engineering, offering a diverse array of applications and a comprehensive range of functionalities.

The FLAC3D software offers a number of advantages, including multi-physics field coupling, dynamic equations of motion solving, and an explicit solution scheme. These features enable the simulation of complex physical processes, such as rock mechanics, heat conduction, and fluid flow, while reducing the required memory space. However, the software requires high input parameters, the solution time is affected by the proportion of natural cycles, and the pre-processing function is relatively limited. Furthermore, FLAC3D boasts a plethora of features, including exclusivity, a command-driven mode, five calculation modes, multiple boundary conditions and structural forms simulations, and openness. The solution process comprises the following steps: modelling, the verification of the static equilibrium, modification of conditions, recalculation until a new equilibrium is reached, the exporting of data, and the analysis of images.

Salt rocks have good creep properties, and the creep deformation of salt rocks is also one of the causes of reservoir instability. FLAC3D software has the function to realise the simulation calculation of five creep material calculation models, so it is necessary to introduce the rheological calculation models of FLAC3D software [26].

2.1.1. WIPP Model

It is essential to consider the effects of time and temperature on the behaviour of salt rock in thermodynamic analyses simulating underground isolation studies of nuclear waste in salt rock. One such model is the WIPP (Waste Isolation Pilot Plant) model. In the FLAC3D finite difference software, the bias strain rate tensor in the WIPP model is composed of a viscous component and an elastic component, which can be expressed as follows:

$$\begin{bmatrix} -d\dot{\varepsilon}_{ij} \\ -d\dot{e}_{ij} \\ -d\dot{\alpha}_{ij} \end{bmatrix} = \begin{bmatrix} \varepsilon_{ij} \\ e_{ij} \\ \alpha_{ij} \end{bmatrix} + \begin{bmatrix} \dot{\varepsilon}_{ij} \\ \dot{e}_{ij} \\ \dot{\alpha}_{ij} \end{bmatrix}, \tag{1}$$

where ε_{ij}, e_{ij}, and α_{ij} are the corresponding strain components; $\dot{\varepsilon}_{ij}$, $\dot{e}_{ij}$, and $\dot{\alpha}_{ij}$ are the corresponding strain rate components; and $\begin{bmatrix} \varepsilon_{ij} \\ e_{ij} \\ \alpha_{ij} \end{bmatrix}$ is the elastic part of the biased strain rate tensor.

The objective of this model is to simulate the time and temperature dependence of the subsurface isolation process of nuclear waste in a salt layer. The FLAC3D software is capable of more accurately describing the complex behaviour of salt rock, including the interaction of the viscous and elastic components, by employing this form of the biased strain rate tensor.

2.1.2. Viscoplastic Model

Viscoelastic models are typically a combination of viscoelastic and plastic models, employed to describe the behaviour of materials during deformation. The WIPP model is a representative viscoelastic model, whereas the Drucker–Prager model is a prevalent plastic model. The combination of these two models provides a more comprehensive description of the deformation behaviour of the material, whereby both viscous and plastic effects are taken into account, thus enhancing the accuracy of the simulation.

The shear yield function for the Drucker–Prager model is shown below:

$$f^s = \tau + q_\phi \sigma_o - k_\phi, \quad (2)$$

where q_ϕ and k_ϕ are the material parameters.

Concurrently, the distinctive attributes and operational procedures of FLAC3D software are integrated with the specific attributes of layered salt-rock underground gas storage reservoirs and the non-linear and creep characteristics of salt rocks. In the simulation, the viscoplastic model is employed for the salt rock layer, while the Moore-Cullen model is utilised for the remaining strata. The objective of employing a combination of models is to provide a more accurate description of the mechanical behaviour of the salt-rock reservoir system. The utilisation of FLAC3D finite-difference software in simulation studies facilitates a more comprehensive comprehension of the long-term stability of salt-rock reservoirs, alongside an evaluation of their viability and safety in practical applications.

2.2. Saltstone Stratigraphic Conditions and Cavity Building Plan

The Pingdingshan Salt Field is rich in mineral deposits, and after nearly 20 years of mining, a large number of abandoned mining cavities have been formed. The salt rocks are distributed in the Cenozoic Paleoproterozoic Loop strata, showing thinly bedded salt rocks and mudstones with alternating lamination, relatively simple tectonics, and horizontal production. The main salt rocks are buried at depths between −1400 and −1000 m [27].

The Pingdingshan salt deposit is a set of Mesozoic and Cenozoic clastic chemical rock series which is contained in the Wuyang Depression. From the Cretaceous to the Quaternary, the Hu Gang Formation (K_2h), Yuhuangding Formation (E_2y), Dacangfang Formation (E_2d), Walnut Garden Formation (E_2h), Liaozhuang Formation (E_3l), Shangshi Formation (N_sh), and Plain Formation (Q_p) were successively deposited. The salt-bearing strata are the nuclear section (top) of the Paleocene Oligocene Walnut Garden Formation. A set of mudstones with a stable distribution is developed at the top of the nuclear section [28]. The profile of the Mesozoic and Cenozoic strata in the Wuyang Depression is shown in Table 1.

Table 1. Sequence stratigraphy list of Wuyang Depression [28].

Stratigraphic System					Thickness/m	Lithologic Association Characteristics
Scope	**Faculty**	**Unite**	**Group**			
Cenozoic K_z	Quaternary Q		Plains group Q_p		25~168	Mottled, light brownish-yellow, lower clay with gravel, middle and upper sandy clay, and clay with several layers of gravel. Unconsolidated contact with underlying strata.
	Neogene Z		Shangji Formation N_sh		300~800	Light yellow, grayish-yellow, and mottled fine conglomerate and conglomerate sandstone are interbedded with grayish-yellow, brownish-red, and grayish-green mudstone. Unconsolidated contact with underlying strata.
	Paleocene system E	Oligocene system E_3	Liaozhuang group E_3l		315~869	Variegated conglomerate sandstone and light gray conglomerate-bearing sandstone are interbedded with brown and grayish-yellow mudstone in consolidated contact with underlying strata.
			Walnut Orchard Group	First nuclear segment E_3h_1	200~1138	The lower part is mudstone, rock salt rock, and cream-bearing mudstone; the middle part is cream-bearing rock salt rock and mudstone; and the upper part is mudstone and cream-bearing mudstone interbedded, sandwiched with rock salt rock. Saltstone is gray and brownish-yellow; other mudstone is gray and brownish-red.
		Eocene system E_2		Second nuclear segment E_2h_2	489~1070	The lower part is dark gray paste-bearing mudstone and mudstone interbedded with fine sandstone, and the bottom is mottled conglomerate sandstone interbedded with purplish-red mudstone; the upper part is gray mudstone, siltstone, oil shale, and grayish-white and brownish-yellow-lithium salts and paste-bearing mudstone.
				Tertiary nuclear segment E_2h_3	784~986	The lower part is grayish-red conglomerate-bearing sandstone, conglomerate sand-stone, light grayish-red fine sandstone, brownish-red, brownish-purple mudstone, locally interspersed with dolomitic mud-stone; the upper part is grayish-red, brownish mudstone, mottled conglomerate sand-stone, and grayish-white greystone.
			Dachangfang Group E_2d		>1200	Variegated sandstone, conglomerate, locally interbedded with brownish-red and purple sandy mudstone and pink-fine sandstone. Consolidated contact with underlying strata.
Cenozoic K_z	Paleocene system E	Eocene system E_2	Yuhuangding Group E_2y		1943	The lower part is brown and purple sand-stone and mudstone interbedded with colourful conglomerate and gray siltstone, etc.; the middle part is purple sandstone, mudstone, and dolomite and marl; and the top part is light gray mudstone, siltstone, and gray–white dolomite.
Mesosphere M_z	Cretaceous K	Unification K_2	Hugang Group K_2h		300	The lower part is yellow–green conglomerate with black coal second layer at the bottom; the upper part is mottled conglomerate in unconformable contact with underlying Carboniferous, Cambrian, or Aurignacian strata.

The sedimentary characteristics and stratigraphic assemblage of the Wulipu salt mine section in Yexian Zhongyan Haolongmazhuang are highly complex. The overall stratigraphy demonstrates a typical lithological sequence comprising alternating salt rocks and mudstones. These are intermixed and distributed, with a large number of intercalated layers, a thin thickness of the single layer, and a deeper burial depth. The geographic location of Ye County is shown in Figure 1.

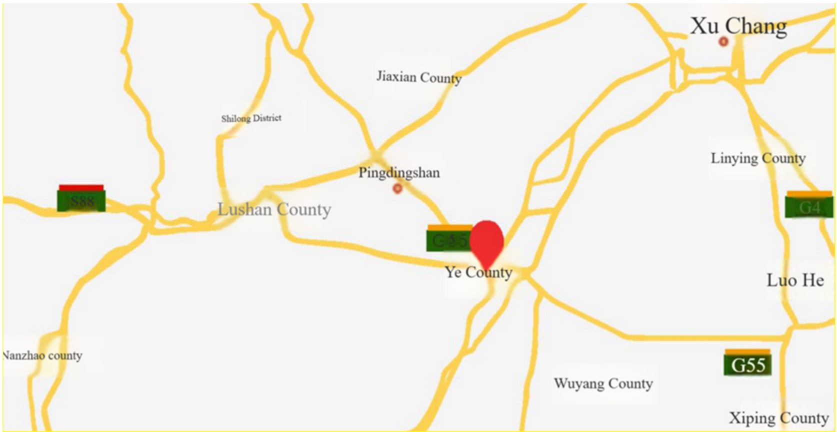

Figure 1. Geographic location map of Ye County, Pingdingshan.

Further investigation reveals that the overall thickness of the salt layers in the Pingdingshan Salt Field region ranges from 489.0 to 1070.0 m, which can be categorised into 22 distinct salt group assemblages, with a maximum of 61 layers reachable. The thickness of a single layer of salt is up to 27.7 m, with the thinnest layers measuring less than 1.0 m, and typically within 10.0 m. The thickness of the mudstone interlayer is variable, with an average of approximately 2.8 m and a maximum of 12.3 m. The majority of the interlayers are within 5 m, representing approximately 30% of the overall thickness.

From a macroscopic perspective, a stable distribution of interlayers is observed at the base of each salt group. In the 0–20 salt group, for instance, the interlayer thickness ranges from 2 to 13.2 m, with an average of 4.1 m. Notably, the interlayer thickness is minimal, reaching a minimum of 0 m. The interlayer thickness at the bottom of the 7, 10, and 13 salt groups is greater than 10 m, with a maximum of 13.2 m. The interlayer thickness in the 14–20 salt groups is 2–8 m, with an average of 5.1 m, and contains eight interlayers in total. In total, there are eight sandwiches.

In order to establish the mechanical model of mudstone entrapment, it is necessary to understand the basic characteristics of the subsurface cavities in detail and obtain relevant data to support the modelling. The consistency of the laboratory simulation studies with the material and joint properties of the field-scale salt cavern conditions helps to improve the relevance and applicability of the studies to real-world engineering, thus providing a reliable guide to real-world engineering applications [29]. Jie Chen and Yichao Rui et al. [30,31]. proposed an acoustic emission positioning technique to effectively reduce the TDOA error by combining the microseismic (MS) source localisation technique and the refraction path study, respectively, which is of good significance for the detection of underground salt cavern gas reservoirs. Wang, Z. R. et al. explored the underground salt cavern gas storage reservoir in Ye County, Pingdingshan, by using the Controlled Source Audio Geomagnetic Method (CSAMT) and the Geodetic Electric Field Petrographic Detection (CYT) method, and obtained the basic features such as the burial depth, dimensions, and spatial location of the underground caverns [32]. According to the summary of Wang, Z. R. et al.'s study, the exploration results show that there are more cavities in the underground of the exploration area, with depths ranging from −1148.0 to −1424.0 m, and with moderate spacing between each other of about 90.0 to 450.0 m. The results are summarised in the following table. The cavity shows a narrow top and wide bottom, with a moderate volume of individual cavities, a range of cavity heights from

153.0 to 233.0 m, averaging about 199.4 m, and a cavity radius between 8.0 and 60.0 m. A schematic of the cavity profile is shown in Figure 2 [33].

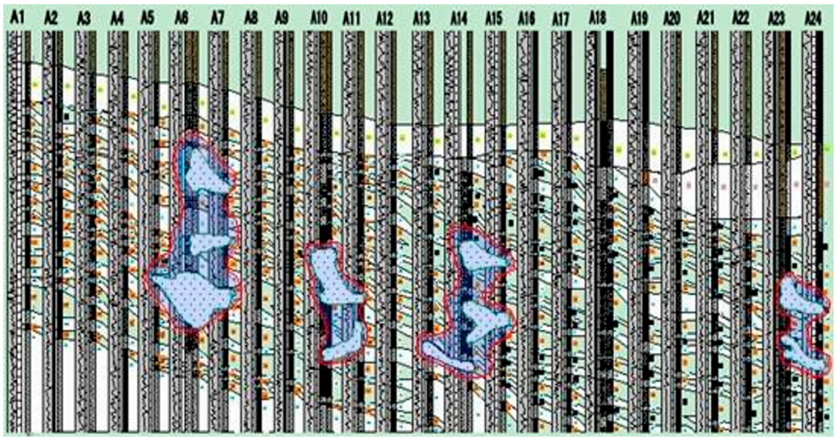

Figure 2. Schematic of underground cavity profile [33].

This paper presents the establishment of a single-cavity model of the salt cavern, created using Ansys 2020R1 and FLAC3D 6.00 software in accordance with the geological conditions observed in the salt cavern gas storage reservoir in Ye County, Pingdingshan. The study concentrated on the impact of varying numbers of mudstone interlayers on displacement changes at the top of the cavity and the volumetric shrinkage rate of the cavity, and presented a summary of the influencing laws. In regard to the long-term safety of salt cavern gas storage reservoirs, it is of paramount importance to select the optimal perimeter rock permeability and operating pressure to effectively prevent deformation resulting from the combined effects of creep and seepage, as well as potential incidents such as cavity instability and gas leakage. In order to facilitate the analysis, an ideal ellipsoidal cavity was constructed. In order to minimise the impact of boundary effects, the model length was set to be between six and eight times the diameter of the cavity. The specific model parameters are set as follows:

All lines (NL1) have a cell boundary size (SIZE) of 2 and a segmentation ratio of 1 (SPACE).

Number 1 (NL1) has a cell boundary size (SIZE) of 2 and is divided into 10 parts (NDIV) with a segmentation ratio of 5 (SPACE).

Control over the cell shape: (1,3D) tetrahedral cell division mesh, (1,2D) triangular division; (0,2D) quadrilateral division, (0,3D) hexahedral division. Tetrahedral cell division mesh is selected.

The grid type for mesh division: 0 free mesh division, 1 mapping mesh division, 2 first choice with mapping, if not, then free mesh division. Free mesh division was chosen.

In this paper, an ellipsoidal cavity will be set up with a long axis of 200 m, a short axis of 100 m, and an aspect ratio of 2. The total length of the model is 1000 m, the width is 500 m, the thickness is 400 m, and the top of the cavity is 1100 m above the surface. Considering the geological data, the 14–20 salt group interlayers were studied and the thickness of the mudstone interlayer was set at 5 m. In order to deeply study the influence law of the number of mudstone interlayers on the long-term operation of the gas storage reservoir, two groups of control experiments will be set up: one group is 6 layers of mudstone interlayers, and the other group is 10 layers of mudstone interlayers.

This design will help to understand the impact of the amount of mudstone entrapment on the long-term operation of a gas storage reservoir. The comparative analysis of the two sets of experiments can reveal more clearly the influence of different numbers of mudstone interlayers on the stability of gas storage reservoirs.

As shown in Figure 3, the storage model schematic shows, in detail, the structure and location distribution of the storage reservoir. In this model, we choose the following key locations as observation points for displacement changes.

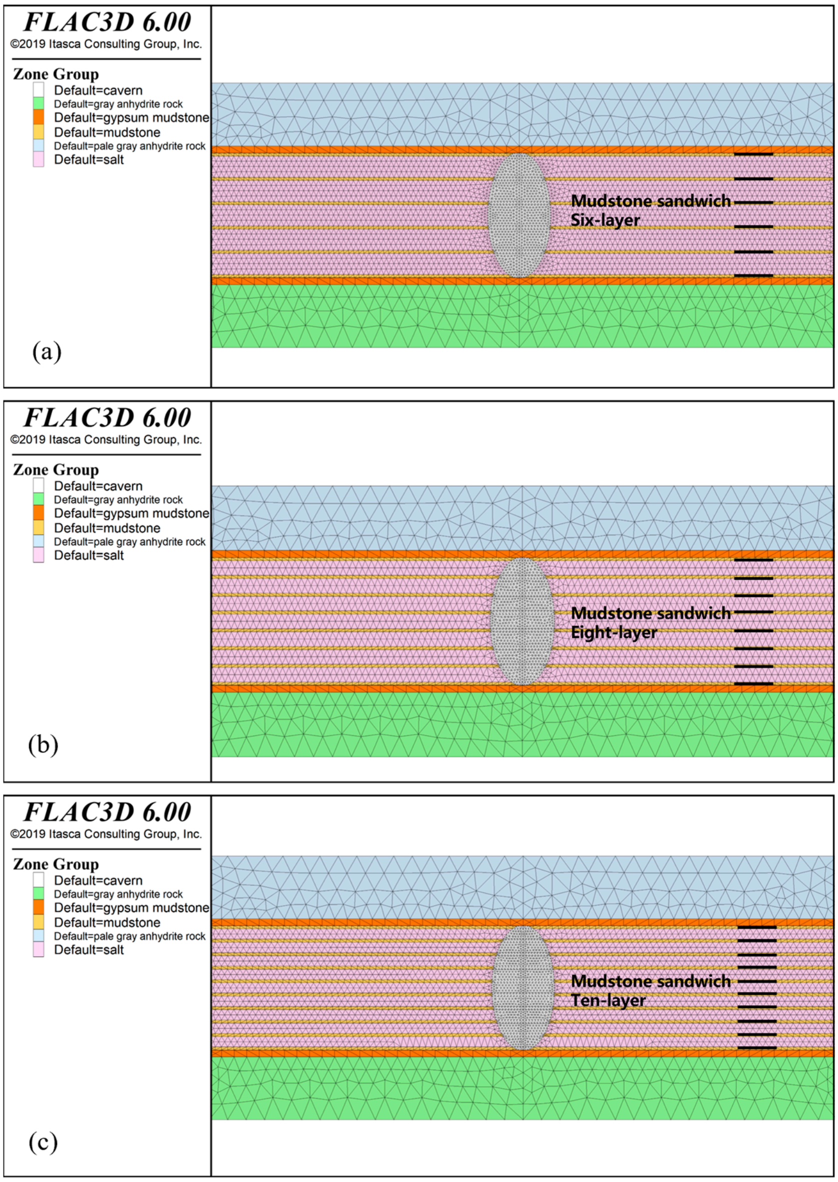

Figure 3. Schematic diagram of the gas storage model: (**a**) Six-layer sandwich; (**b**) Eight-layer sandwich; (**c**) Ten-layer sandwich.

Top Plate Position (T): This is the top position of the model, above the cavity. Monitoring displacement changes at this point can help assess the stability of the roof and potential risk of collapse.

Left position of the cavity side gang (L): this is the position on the left side of the cavity, and monitoring displacement changes at this point can provide information on lateral stresses and deformations.

Right position of the cavity side gang (R): this is the position on the right side of the cavity, corresponding to the left position, and it is equally important to monitor displacement changes at this point to get a full picture of lateral stresses and deformations.

Baseplate position (B): This is the bottom position of the model, located below the cavity. Monitoring displacement changes at this point helps to assess the stability of the footing and potential subsidence or uplift.

The data from these observation points can provide a comprehensive understanding of the displacement changes in different parts of the gas storage reservoir during long-term operation, thus providing an important reference for the safe operation and structural optimisation of the gas storage reservoir. Firstly, the construction of the cavity model was carried out, and subsequently, the mechanical parameters were set in FLAC3D to determine the computational parameters for the creep properties of the rock [34,35], as shown in Table 2. (In the context of salt mines, the aforementioned data are considered standard and are subject to testing at the mine level. The data presented in Table 2 have been sourced from the mine's operational documentation).

Table 2. Physical parameters of rock layer.

Rock Mass	Bulk Modulus/GPa	Shear Modulus/GPa	Cohesive Force/MPa	Tensile Strength/MPa	Internal Friction Angle/°
salt rock	8.67	3.95	1.93	1.20	37.5
sandstone	13.04	6.81	2.9	1.6	36
mud rock	13.04	6.81	2.9	1.60	36
Calcareous	8.45	3.85	0.50	0.50	30.0
gypsum rock	10.92	5.54	2.2	1.4	35
Light gray	13.04	6.81	2.9	1.6	36
anhydrite rock	13.04	6.81	2.9	1.60	36

The initial and boundary conditions of the reservoir cavity have an important influence on the mechanical characterisation of salt cavern reservoirs. According to the research of related scholars, a certain consensus exists on the value of the air pressure cycle in the cavity of the gas storage reservoir, i.e., it is believed that the value of the pressure during the air pressure cycle should be limited to 0.3–0.8 times that of the geopathic stress in the vertical direction. Studies have shown [36] that the main factor affecting the long-term stable operation of gas storage reservoirs is low pressure, so related scholars have proposed that the minimum air pressure is set at 33% or more. Considering multiple factors, the range of circulating gas pressure in the reservoir was finally determined to be 0.3–0.8 times the vertical geopathic stress (10–22 MPa) [37–39]. In this paper, the range of cyclic air pressure is set to be 12–18 MPa, and the main manifestations of single salt cavern cavity destabilisation include roof failure and cavity deformation, while the stability of the sidewalls needs to be considered as well [40–42]. In this study, three sets of tests were conducted: a 6-layer mudstone entrapment, an 8-layer mudstone entrapment, and a 10-layer mudstone entrapment. By comparing the displacement changes of the top and bottom plates and sidewalls, as well as the volume shrinkage rate, in these three sets of tests, it is possible to discuss the influence of different numbers of mudstone interlayers on the long-term operation of gas storage reservoirs. The aforementioned test setup can facilitate an understanding of the stability performance of salt caverns under different numbers of entrapment conditions, thereby providing a valuable reference point for the design and operation of gas storage facilities. By monitoring the alterations to the top and sidewalls of the salt caverns, it is possible to ascertain the degree to which varying quantities of mudstone entrapment influence the stability of the salt caverns. This enables the formulation of more logical operational and management strategies.

3. Results

After simulating the 30-year operation of a vertical single-cavity gas storage reservoir in FLAC3D, and after the calculation by FLAC3D software, we obtained the displacement maps of the salt cavities under cyclic gas pressure for different numbers of mudstone interlayers. As the operating time increases, the displacement distribution of the surrounding rock changes, especially the vertical and horizontal displacements. Figure 3 illustrates the cloudy distribution of the vertical displacement of the surrounding rock after 1, 5, 10, 15, 20, and 30 years of operation for a single-cavity vertical gas storage reservoir with a number of eight interlayers, while Figure 4 illustrates the cloudy distribution of the horizontal displacement of the surrounding rock for the same reservoir over the same period of time.

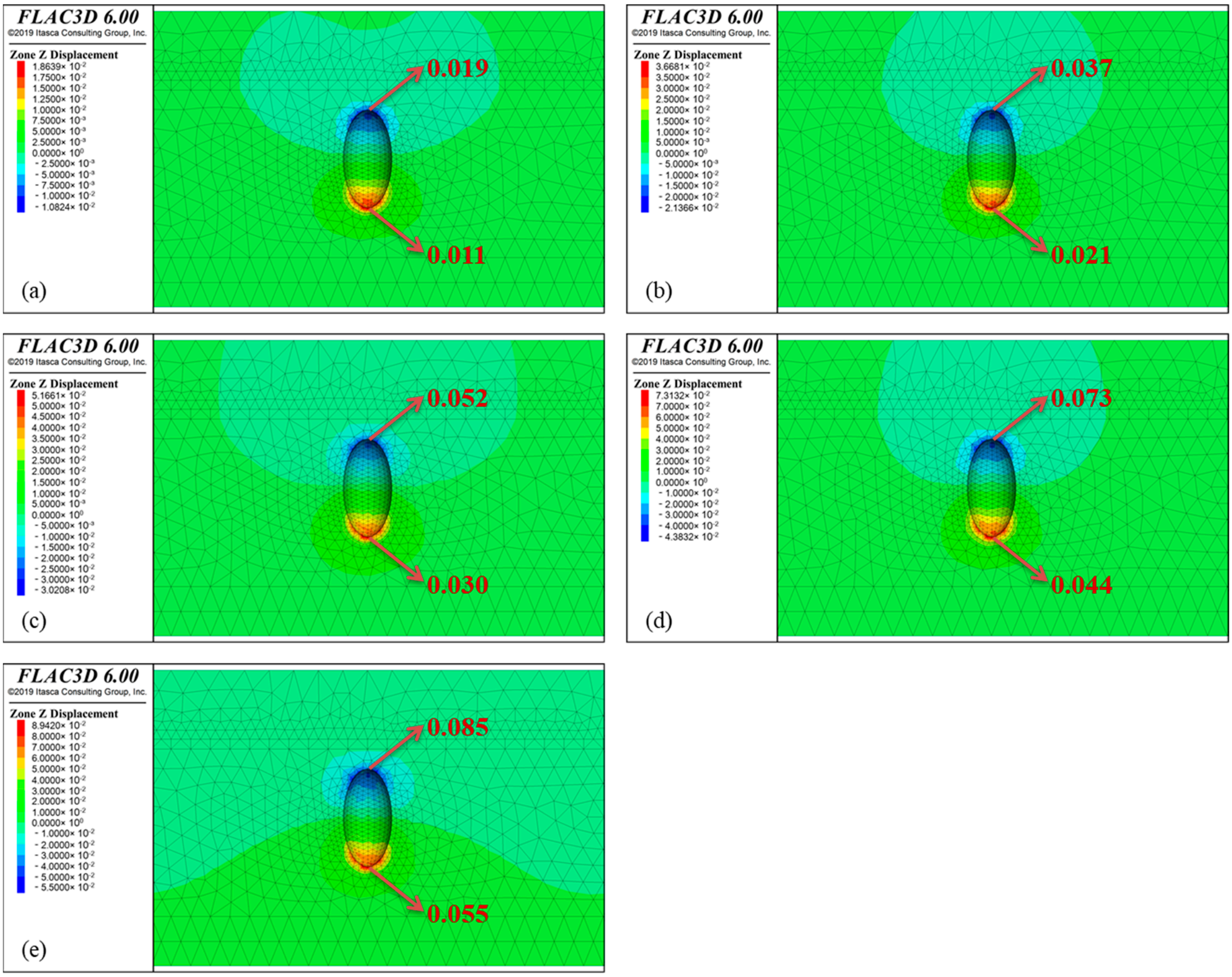

Figure 4. Vertical displacement of the surrounding rock of a single-cavity vertical gas storage reservoir with time: (**a**) One year; (**b**) Five years; (**c**) Ten years; (**d**) Twenty years; (**e**) Thirty years.

The plots offer valuable insights into the temporal displacement of the gas storage enclosure. The observation of displacement cloud maps at varying time points allows for the comprehension of the deformation of the surrounding rock during the operation of the gas storage reservoir.

A detailed examination of the test results reveals that the cavities under different numbers of mudstone interlayers all exhibit a contraction towards the interior. In contrast, the deformation of the upper surface of the cavity is consistently greater than that of the lower surface, and a symmetrical tendency is observed on the lateral walls. This phenomenon can be attributed to the fact that the cavity is situated in a gradient distribution of low stress states, with high-pressure gases filling the cavity and exhibiting an isobaric distribution. Consequently, the top and bottom of the force are not uniform.

The gradient distribution of ground stress causes the ground stress on the top of the cavity to potentially be greater than that on the bottom, so the deformation of the top will be relatively larger. And the high-pressure gas is distributed as isobaric inside the cavity, which means that the stress state inside the cavity is uniform. However, the ends of the cavity are in a state of uneven stress and may have been subjected to greater stresses, so the deformation at the ends of the cavity will be greater.

In addition, the further away the surrounding rock is from the cavity, the less it is affected, but by and large, it shows a symmetrical distribution up and down along the short axis of the cavity. This is because the surrounding rock away from the cavity is less affected, but the deformation of the cavity will affect the surrounding rock, so that the deformation along the short axis of the cavity presents a symmetrical distribution on the whole. Thus, these factors combine to characterise the deformation of the cavity under different conditions.

As illustrated in Figure 4, the vertical displacement of the surrounding rock of the vertical single-cavity gas storage reservoir is increasing over time. To illustrate, the settlement value at the upper limit of the reservoir increased from 0.019 m to 0.089 m over the course of 30 years, while the maximum uplift value at the lower limit rose from 0.011 m to 0.055 m over the same period.

By observing the vertical displacement cloud diagram of the surrounding rock of the gas storage reservoir in Figure 4, it is found that with the increase in time, the maximum settlement value of the surrounding rock at the top of the reservoir is always larger than the maximum uplift value at the bottom of the reservoir, e.g., the maximum settlement value of the top of the single-cavity reservoir with eight layers of mudstone interlayers after 30 years of operation is 0.089 m, and the maximum uplift value of the bottom of the reservoir is 0.055 m. The asymmetry in the vertical displacement of the gas reservoir envelope is due to the different effects of creep action on the top and bottom of the reservoir.

During the operation of a gas storage reservoir, there may be differences in the stresses and temperatures to which the top and bottom are subjected, which could result in disparate creep effects between the two. The upper portion of the reservoir may experience greater stress levels than the lower portion. Furthermore, given that temperature typically increases gradually with depth, the temperature at the bottom may be higher than at the top, resulting in disparate creep effects.

Thus, the fact that the maximum settlement value at the top of the gas storage enclosure is consistently greater than the maximum bulge value at the bottom over time is due to the different effects of creep on the top and bottom of the storage reservoir.

The horizontal displacement cloud map of the surrounding rock after 30 years of operation was obtained by numerical simulations for the vertical single-cavity salt rock reservoir with eight layers of mudstone interlayers, as illustrated in Figure 5. The remaining models exhibited comparable patterns.

Figure 5 illustrates that the horizontal displacement of the surrounding rock in the single-cavity vertical gas storage reservoir is influenced by the surrounding pressure, with a tendency for expansion into the cavity. This suggests that the surrounding rock has undergone horizontal deformation in the direction of inward contraction, which has resulted in a reduction in the effective volume of the gas storage reservoir.

At the same time, the horizontal displacement of the enclosing rock shows a clear symmetry with respect to the vertical displacement of the top and bottom of the enclosing rock. This means that the maximum value of the displacement change towards the interior of the cavity at the horizontal ends is approximately equal. For example, the horizontal displacement values at the horizontal ends of the reservoir in year 30 are 0.1149 m and 0.1227 m. This symmetry may be attributed to the deformation of the surrounding rocks occurring horizontally under the influence of similar geologic stresses and confining pressures, which results in the deformation of the surrounding rocks occurring horizontally showing a similar tendency at the two ends.

A summary the variation of perimeter rock displacement with time for a single-cavity vertical gas storage reservoir is shown in the Figure 6. Overall, these observations help to understand the deformation characteristics of the gas storage enclosure rock when subjected to subsurface pressure, which is of great engineering significance for the design and management of gas storage reservoirs.

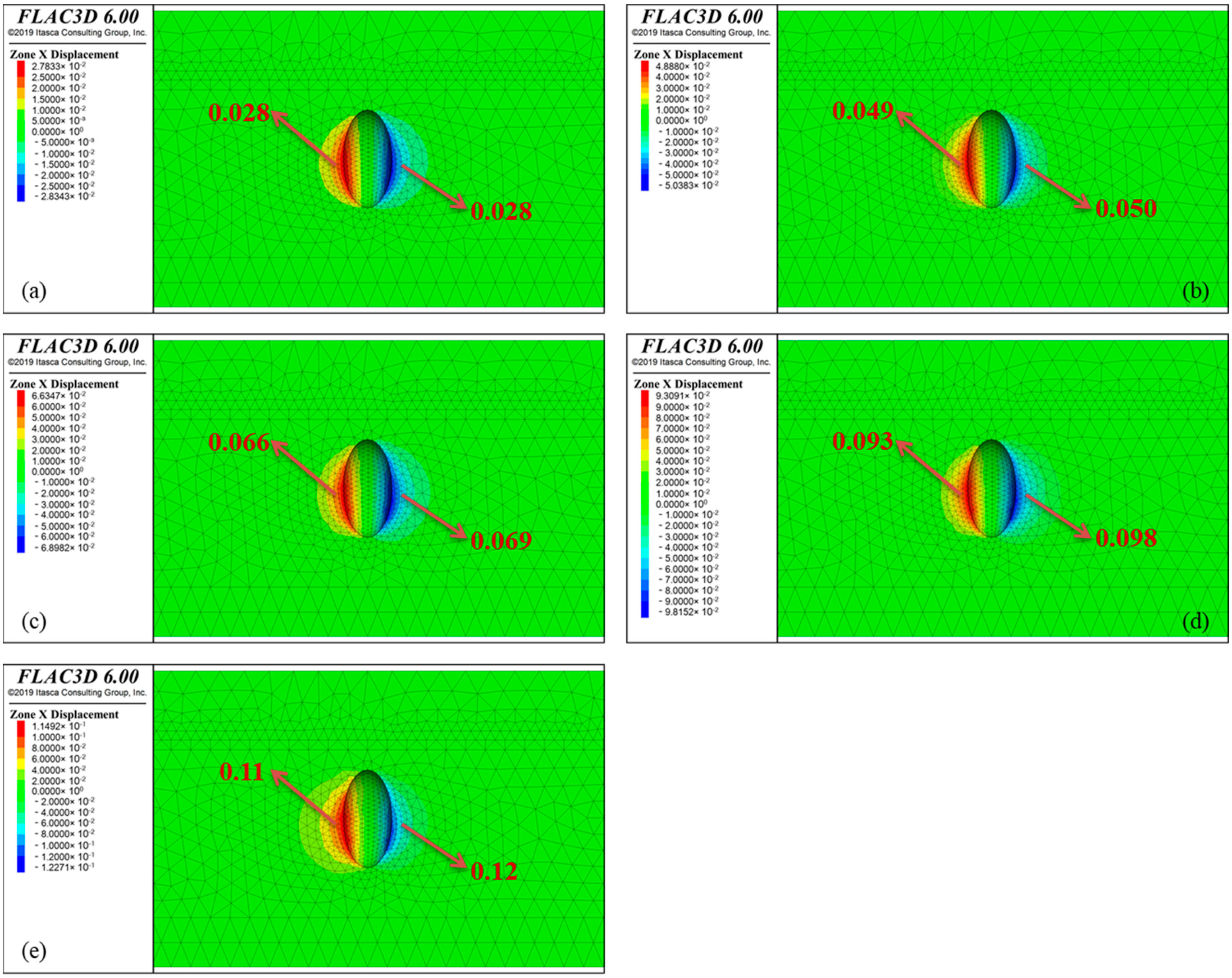

Figure 5. Horizontal displacement of the surrounding rock of a single-cavity vertical gas storage reservoir with time: (**a**) One year; (**b**) Five years; (**c**) Ten years; (**d**) Twenty years; (**e**) Thirty years.

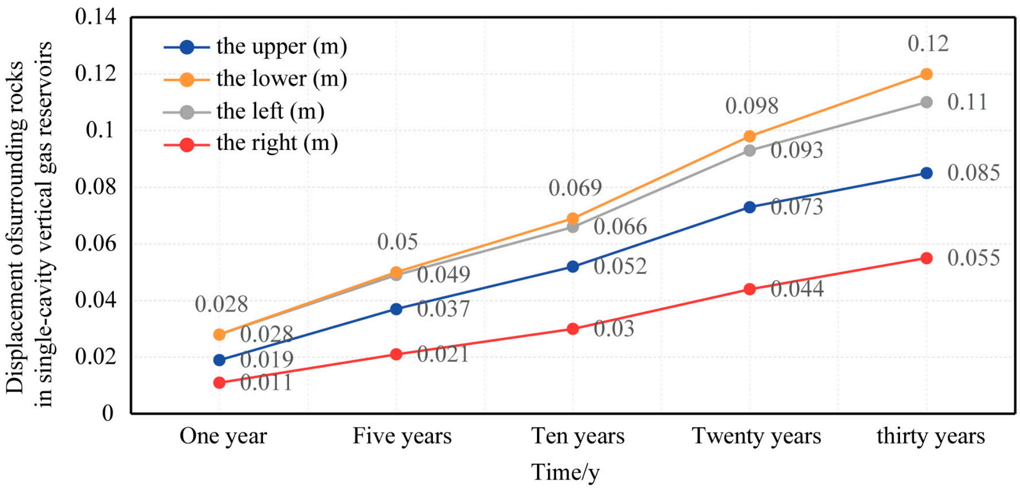

Figure 6. Plot of perimeter rock displacement versus time for a single-cavity vertical gas reservoir.

4. Discussion

The data pertaining to displacement, obtained from the numerical simulation of single-cavity vertical gas storage reservoir monitoring points, were subjected to processing using Origin 2018 software, with the objective of obtaining the rule of change.

The changes in vertical displacement at monitoring points T and B and the top and bottom plates of the cavity are shown in Figure 5, respectively.

From Figure 7, a trend can be clearly observed: as the number of mudstone interlayers increases, the displacement of the top and bottom plates of the reservoir increases. This trend reflects the relatively weaker nature of the mudstone interlayer in the surrounding rock. The increase in the number of interlayers under the same cyclic air pressure directly leads to an increase in displacement deformation.

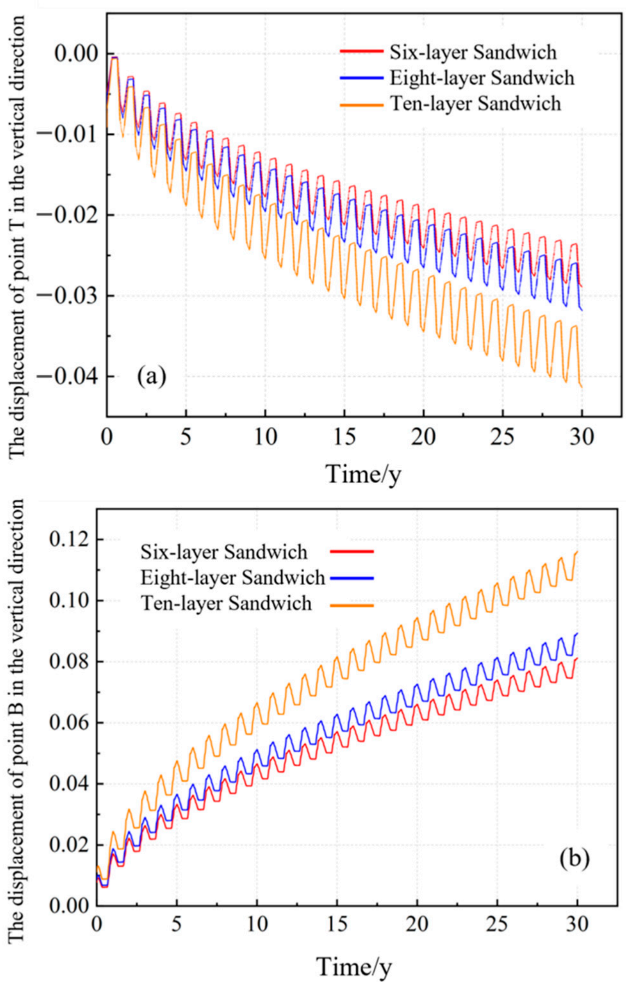

Figure 7. Vertical Displacement of Monitoring Points T and B: (**a**) The top plate; (**b**) The base plate slab.

The explanation for this phenomenon can be attributed to the role of mudstone interlayers in the reservoir structure. Mudstone interlayers typically have lower strength and higher deformability and are, therefore, more susceptible to displacement and deformation when subjected to external pressures. When the number of mudstone entrapments increases, the relative proportion of mudstone entrapment in the gas storage structure increases, and the effects of their displacement and deformation increase accordingly.

It is, therefore, imperative that the impact of the quantity of mudstone inclusions on the stability of the surrounding rock is given due consideration at all stages of the design and operational phases of a gas storage reservoir. Appropriate support and reinforcement measures are implemented to mitigate the adverse effects of mudstone interlayers on the structural stability of gas storage reservoirs, thereby ensuring the safe operation of the reservoirs. These findings have significant implications for the optimisation of reservoir operation strategies, the reduction of surrounding rock deformation, and the improvement of long-term reservoir stability. The deformation of the surrounding rock can be effectively mitigated through the implementation of a rationalised air pressure peaking strategy and the regulation of the air pressure action time, thereby enhancing the performance and safety of the gas storage reservoir.

From Figure 8, the changes in horizontal displacement show a similar pattern to the vertical displacement, which is due to the contraction of the cavity under the influence of the circulating air pressure. It is worth noting that the displacement changes on the left and right sides are nearly symmetrical, which means that the trend of changes on the left and right sides is similar when the cavity is affected. Similar to the vertical displacement, the effect of the number of interlayers on the horizontal displacement change is also consistent. When the number of mudstone inclusions is increased, it leads to greater horizontal displacement changes, which suggests a positive correlation between the number of inclusions and displacement changes.

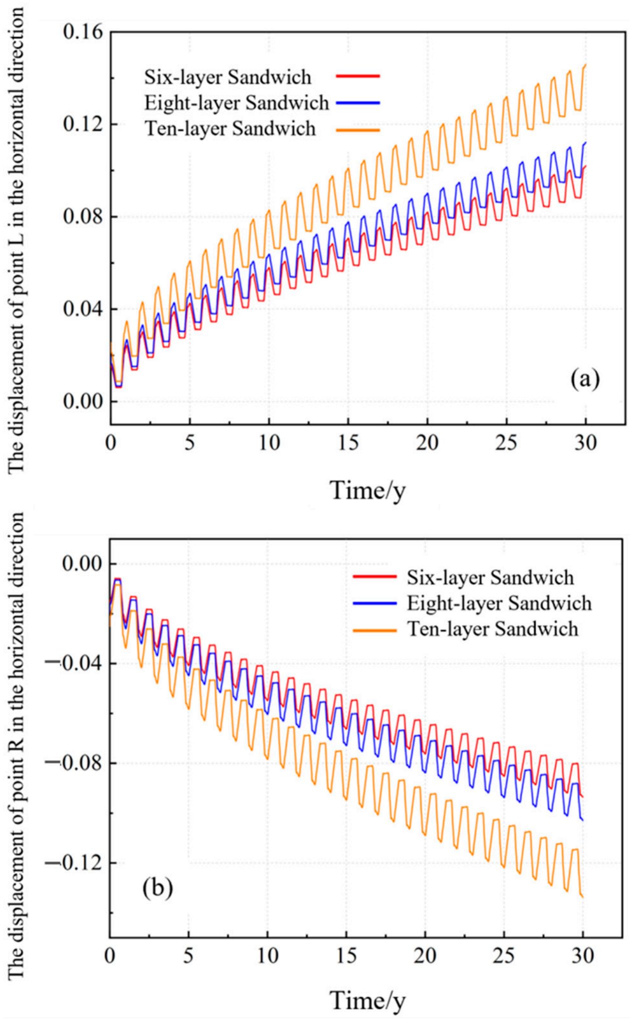

Figure 8. Horizontal Displacement of Monitoring Points L and R: (**a**) The left plate; (**b**) The right plate slab.

The volumetric shrinkage of a cavity is defined as the extent to which its volume decreases due to deformation of the surrounding rock under specific conditions. The volume change of the cavity is calculated and monitored using FLAC3D, and the resulting data are instrumental in comprehending the deformation of the cavity under disparate operational conditions, as well as in appraising the stability and performance of the gas storage reservoir. Figure 9 illustrates the variation in cavity volume shrinkage at different air pressure cycling frequencies.

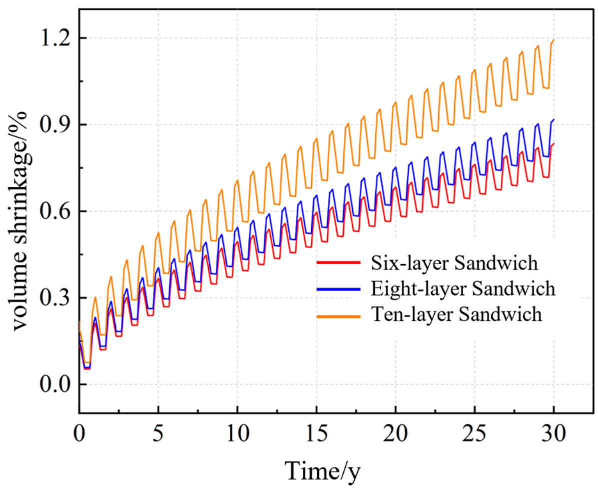

Figure 9. Volume shrinkage with time at different intervals.

As can be seen from the above figure, the volumetric shrinkage of the gas storage reservoirs all show a nearly exponential and steady increase for different numbers of mudstone interlayers. This trend suggests that the rate of the volumetric shrinkage of the reservoir does not change linearly over time and with the continued action of the circulating air pressure, but rather increases gradually at a faster rate, especially if the number of interlayers is high.

The exponential increase in volumetric shrinkage indicates that the mudstone interlayer plays a pivotal role in the long-term operation of the reservoir. The increase in the number of mudstone interlayers not only results in an increase in the displacement and deformation of the surrounding rocks, but also presents the gas storage reservoir face with greater challenges in terms of its overall stability. In particular, as the number of mudstone interlayers rises, the intricacy of the reservoir's internal configuration intensifies, and the mechanical interconnections between the layers become more pronounced. This renders the reservoir more vulnerable to deformation when subjected to pressure, and consequently, volumetric shrinkage is accelerated.

This phenomenon places higher demands on the design and management of gas storage reservoirs. In order to slow down the exponential growth of volumetric shrinkage, it is necessary to carry out fine geological investigations and mechanical analyses at the early stage of gas storage reservoir construction. Meanwhile, during the operation of the gas storage reservoir, it is necessary to regularly monitor the volume changes and perimeter rock deformation, and take timely remedial measures, such as adjusting the circulating air pressure and strengthening the support structure, in order to maintain the long-term stability and safety of the gas storage reservoir.

Figure 10 shows the plastic zone volume for a single cavity vertical gas storage. In this figure, it can be observed that the plastic zone volume is, overall, small with a maximum value of only 1 m^3. This smaller plastic zone volume may be due to the fact that the reservoirs are designed for a long service life, usually more than 30 years, and also have long injection and extraction cycles with very stable pressures in the chamber.

Furthermore, the volume of the plastic zone demonstrates a persistent augmentation with time for varying numbers of interlayers, exhibiting a consistently accelerating growth rate. This indicates that the volume of the plastic zone will increase gradually and at an accelerated rate as the reservoir is operated over time.

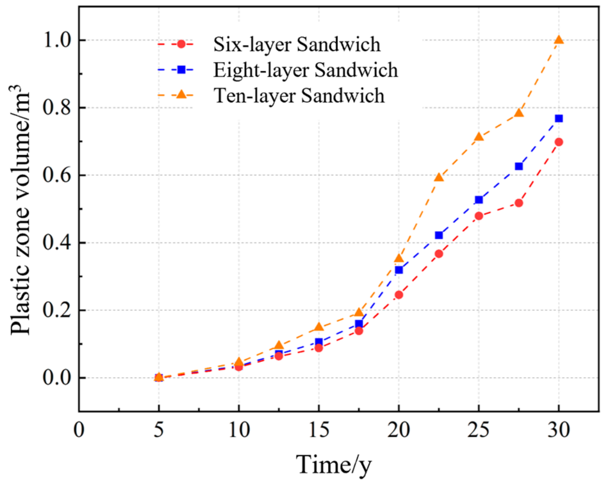

Figure 10. Plastic zone volume variation with interval time.

5. Conclusions

In view of the special geological conditions of layered salt rocks in China, and in order to deeply investigate the influence of the number of mudstone interlayers on the long-term safe and stable operation of gas storage reservoirs, this study conducted numerical simulation analyses of gas storage reservoirs containing 6, 8, and 10 layers of mudstone interlayers, respectively, and came up with the following main conclusions.

(1) As the number of mudstone interlayers increases, the vertical displacement of the surrounding rocks of the vertical single-cavity gas storage reservoir also increases. This is evidenced by the observation that the maximum settlement value at the upper boundary of the gas storage enclosure is consistently less than the maximum uplift value at the lower boundary. This asymmetry in vertical displacement is primarily attributable to discrepancies in ground stresses stemming from the disparate depths at which the top and bottom slabs are situated. The top is subjected to less geopathic stress, whereas the bottom is subjected to higher geopathic stress, which results in a greater tendency for the surrounding rock at the bottom to undergo uplift, given that it bears the weight of the reservoir. This asymmetry is a reflection of the impact of a stratigraphic depth on the distribution of ground stress, and is a principal factor contributing to the observed differences in the vertical displacement of the surrounding rocks of the gas storage reservoir.

(2) The horizontal displacement exhibits a clear symmetry. In comparison with the vertical displacement observed at the top and bottom of the surrounding rock formation, the horizontal displacement of the surrounding rock formation demonstrates a distinct symmetry. This symmetry may be attributed to the resemblance in geological stress and confining pressure within the gas reservoir, which gives rise to the horizontal deformation of the surrounding rock exhibiting analogous trends at both ends. This finding demonstrates that, when subjected to horizontal stress, an increase in the interlayer does not result in the destruction of the symmetry of horizontal displacement.

(3) The influence of circulating air pressure on the horizontal displacement of surrounding rock is consistent with its influence on vertical displacement. An increase in the number of mudstone entrapments leads to greater horizontal displacement changes. This implies that an increase in the number of interlayers will further amplify the amplitude of the horizontal displacement of the surrounding rock under cyclic gas pressure, indicating that the number of interlayers has an important influence on the stability of the gas reservoir.

(4) A change in the volume of the plastic zone was observed. It was determined that the volume of the plastic zone within the gas storage reservoir is relatively limited in scope. However, the rate of contraction for the reservoir demonstrates a notable exponential and consistent increase over time. The volume of the plastic zone continues to increase with time for different numbers of interlayers, and the rate of increase continues to accelerate.

This trend indicates that the number of interlayers has a considerable impact on the plastic deformation of the surrounding rocks of the reservoir. Consequently, an increase in the number of interlayers results in a proportional acceleration in the expansion rate of the plastic zone volume, which in turn exerts a more pronounced influence on the long-term stability of the reservoir.

Author Contributions: Conceptualization, L.L.; Methodology, X.J.; Software, J.T. and J.S.; Formal analysis, R.L.; Resources, X.Q.; Project administration, J.F. and C.Q. All authors have read and agreed to the published version of the manuscript.

Funding: This work was supported by Chongqing Science and Technology Bureau (CSTB2022NSCQ-MSX1595).

Institutional Review Board Statement: Not applicable.

Informed Consent Statement: Not applicable.

Data Availability Statement: The data presented in this study are available on request from the corresponding author. The data is not publicly available due to privacy.

Conflicts of Interest: Authors Lilong Li and Xiaolinag Quan were employed by the company Sichuan Yanjiang Yijin Expressway Co., Ltd.; Authors Xin Jiang and Cheng Qian were employed by the company Chongqing Chengtou Jiangchang Construction Co., Ltd. The remaining authors declare that the research was conducted in the absence of any commercial or financial relationships that could be construed as a potential conflict of interest.

References

1. Wanyan, Q. *Evaluation of Geological Conditions and Countermeasures for Salt Cavern Underground Gas Storage in China*; Southwest Petroleum University: Chengdu, China, 2015.
2. Guo, B.; Fang, D.; Wang, X.; Zhang, S. Development of technology of salt cavern underground natural gas storage in foreign countries. *Fault Block Oil Field* **2002**, *1*, 78–80+86.
3. Wang, Z.; Yuan, G.; Ban, F. Experimental study on the utilization of sediment space in salt cavern gas storage in butt well. *Chin. Mine Salt* **2020**, *51*, 27–30.
4. Yang, C.; Wang, T. Progress in deep earth energy storage research. *J. Rock Mech. Eng.* **2022**, *41*, 1729–1759.
5. Ren, P.; Qi, L.; Wang, W.; Jiao, Y.; Zhou, Z.; Wang, W. Current status and development trend of space utilisation in salt caverns. *Oil Gas Field Surf. Eng.* **2023**, *42*, 1–8.
6. Chen, J.; Jiang, D.; Liu, W.; Huang, G.; Fan, J. Progress of water-soluble cavity creation and comprehensive utilisation of cavities in salt mines. *China Sci. Found.* **2021**, *35*, 911–916.
7. Taheri, S.; Pak, A.; Shad, S.; Mehrgini, B.; Razifar, M. Investigation of rock salt layer creep and its effects on casing collapse. *Int. J. Min. Sci. Technol.* **2020**, *30*, 357–365. [CrossRef]
8. Zhao, K.; Li, H.; Ma, H.; Yu, H.; Li, H.; Zeng, Z.; Zheng, Z.; Chen, X.; Yang, C. Creep-fatigue characteristics of rock salt under different loading paths. *J. Pet. Sci. Eng.* **2022**, *218*, 111036. [CrossRef]
9. Ma, L.; Wang, Y.; Wang, M.; Xue, B.; Duan, L. Mechanical properties of rock salt under combined creep and fatigue. *Int. J. Rock Mech. Min. Sci.* **2021**, *141*, 104654. [CrossRef]
10. Ozsen, H.; Ozkan, I.; Sensogut, C. Measurement and mathematical modelling of the creep behaviour of Tuzköy rock salt. *Int. J. Rock Mech. Min. Sci.* **2014**, *66*, 128–135. [CrossRef]
11. Wang, J.; Liu, X.; Huang, M.; Yang, X. Analysis of axial creep of salt rock under low frequency cyclic loading by Burgers model. *Rock Soil Mech.* **2014**, *35*, 933–942.
12. Jiang, D.; Fan, J.; Chen, J.; Yang, C.; Chui, Y. Effect of intermittent fatigue test on fatigue characteristics of salt rock. *J. Geotech. Eng.* **2016**, *38*, 1181–1186.
13. Fan, J.; Tang, L.; Chen, J.; Yang, Z.; Jiang, D. Creep fatigue constitutive model of salt rock based on hardening parameters. *Rock Soil Mech.* **2023**, *44*, 1271–1283.
14. Li, Z.; Jiang, D.; Fan, J.; Chen, J.; Liu, W.; Wu, F.; Du, C.; Kang, Y. Experimental study on fatigue characteristics of salt rock at triaxial interval. *Rock Soil Mech.* **2020**, *41*, 1305–1312.
15. Chui, Y.; Jiang, D.; Du, F.; Chen, J.; Ren, S.; Fan, J. Experimental study on acoustic emission characteristics of salt rock interval fatigue. *J. Cent. South Univ. (Nat. Sci. Ed.)* **2017**, *48*, 1875–1882.
16. Li, X.; Sun, X.; Xu, Q.; Liu, B. Experimental study on fatigue characteristics of rock salt under the influence of time interval. *J. Undergr. Space Eng.* **2017**, *13*, 606–611.
17. Hou, B.; Shangguan, S.; Niu, Y.; Su, Y.; Yu., C.; Liu, X.; Li, Z.; Li, J.; Liu, X.; Zhao, K. Unique properties of rock salt and application of salt caverns on underground energy storage: A mini review. *Energy Sources Part A Recovery Util. Environ. Eff.* **2024**, *46*, 621–635. [CrossRef]

18. Yu, H.; Ji, W.; Hou, J.; Shang, H.; Wan, J.; Ma, H. Stability study of a compressed air energy storage power station with shallow buried salt caverns. *Electr. Surv. Des.* **2024**, *3*, 69–75.
19. Liang, W.; Tang, L.; Li, X.; Chen, G.; Jiang, D. Stability analysis of near-field perimeter rock for salt cavern pressurised gas storage reservoirs. *J. Undergr. Space Eng.* **2023**, *19*, 698–706.
20. Fu, X.; Xia, Y.; Xu, Z.; Yuan, G.; Ban, F. Numerical simulation of the stability of compressed air energy storage cavities in salt caverns. *J. Undergr. Space Eng.* **2018**, *14*, 930–934.
21. Liu, W.; Zhang, Z.; Chen, J.; Jiang, D.; Wei, F.; Fan, J.; Li, Y. Feasibility evaluation of large-scale underground hydrogen storage in bedded salt rocks of China: A case study in Jiangsu province. *Energy* **2020**, *198*, 117348. [CrossRef]
22. Zhang, Z.; Liu, W.; Guo, Q.; Duan, X.; Li, Y.; Wang, T. Tightness evaluation and countermeasures for hydrogen storage salt cavern contains various lithological interlayers. *J. Energy Storage* **2022**, *50*, 104454. [CrossRef]
23. Yang, C.; Wang, T.; Chen, H. Theoretical and Technological Challenges of Deep Underground Energy Storage in China. *Engineering* **2023**, *25*, 168–181. [CrossRef]
24. Wang, T.; Ding, Z.; He, T.; Xie, D.; Liao, Y.; Chen, J.; Zhu, K. Stability of the horizontal salt cavern used for different energy storage under varying geological conditions. *J. Energy Storage* **2024**, *84*, 110817. [CrossRef]
25. Lankof, L.; Tarkowski, R. GIS-based analysis of rock salt deposits' suitability for underground hydrogen storage. *Int. J. Hydrogen. Energy* **2023**, *48*, 27748–27765. [CrossRef]
26. Bai, X. *Stability Analysis of Horizontal Oil Storage Groups in Stratified Salt Rock*; Chongqing University: Chongqing, China, 2022.
27. Wang, Z.; Li, Y.; Zhang, L.; Chen, L. Engineering geological conditions and feasibility analysis of thin bedded salt rock underground gas storage. *J. Eng. Geol.* **2015**, *23*, 148–154.
28. Chen, B.; Shen, X.; Wanyan, Q.; Sun, L. Geological condition evaluation of Pingdingshan salt cavern gas storage. *Sci. Technol. Guide* **2016**, *34*, 135–141.
29. Chen, J.; Tong, J.; Rui, Y.; Cui, Z.; Pu, Y.; Du, J.; Derek, B.A. Step-path failure mechanism and stability analysis of water-bearing rock slopes based on particle flow simulation. *Theor. Appl. Fract. Mech.* **2024**, *131*, 104370. [CrossRef]
30. Chen, J.; Chen, J.; Rui, Y.; Pu, Y. Joint Inversion of AE/MS Sources and Velocity with Full Measurements and Residual Estimation. *Rock Mech. Rock Eng.* **2024**, *57*, 7371–7386. [CrossRef]
31. Rui, Y.; Chen, J.; Chen, J.; Qiu, J.; Zhou, Z.; Wang, W.; Fan, J. A robust triaxial localization method of AE source using refraction path. *Int. J. Min. Sci. Technol.* **2024**, *34*, 521–530. [CrossRef]
32. Wang, Z.; Wang, Q.; Zhang, L. Application of CSAMT and CYT combined detection method in the construction of deep salt cavern gas storage. *J. Eng. Geol.* **2016**, *24*, 142–149. [CrossRef]
33. Wang, Y. *Study on the Stability and Collapse Disaster of Interlayer of Pingdingshan Salt Cavern Gas Storage*; Zhengzhou University: Zhengzhou, China, 2019.
34. Xiao, Y.; Xu, M. FLAC(3D) and ANSYS modeling characteristics and their applications. *Hydropower Technol. Gansu* **2011**, *47*, 11–12.
35. Zhang, G.; Wang, L.; Wu, Y.; Li, Y.; Yu, S. Failure mechanism of bedded salt formations surrounding salt caverns for underground gas storage. *Bull. Eng. Geol. Environ.* **2017**, *76*, 1609–1625. [CrossRef]
36. Jiang, D.; Wang, Y.; Liu, W.; Li, L.; Qiao, W.; Chen, J.; Li, D.; Li, Z.; Fan, J. Construction simulation of large-spacing-two-well salt cavern with gas blanket and stability evaluation of cavern for gas storage. *J. Energy Storage* **2022**, *48*, 103932. [CrossRef]
37. Liu, W.; Chen, J.; Jiang, D.; Shi, X.; Li, Y.; Daemen, J.J.K.; Yang, C. Tightness and suitability evaluation of abandoned salt caverns served as hydrocarbon energies storage under adverse geological conditions (AGC). *Appl. Energy* **2016**, *178*, 703–720.
38. Yang, C.; Zhou, H.; Li, Y. *Disaster Mechanism and Protection of Large Salt Cavern Gas Storage Group*, 3rd ed.; Science Press: Beijing, China, 2014.
39. Zhang, G.; Wang, Z.; Liu, W.; Luo, L.; Dong, J. Study on stability of key roof of compressed air energy storage in horizontal salt cavern. *Rock Soil Mech.* **2021**, *42*, 800–812.
40. Xu, S.; Zhang, Q.; Li, X.; Gai, Z.; Wen, P.; Wei, Q. Research on optimization design of injection and production operation parameters of Jintan Salt Cave gas storage. *Oil Drill. Prod. Technol.* **2020**, *42*, 490–496.
41. Jing, W.; Yang, C.; Li, L.; Yuan, Z.; Shi, X.; Li, Y. Sensitivity analysis of factors affecting shrinkage risk of salt cavern gas storage. *J. Rock Mech. Eng.* **2012**, *31*, 1804–1812.
42. Tang, Z.; Jiang, D.; Chen, J.; Fan, J.; Liu, W. Comprehensive evaluation on stability of salt cavern storage with small well spacing and double well spacing. *J. Undergr. Space Eng.* **2021**, *17*, 1997–2006.